EXAFS Study of Dopant Segregation (Zn, Nb) in Nanocrystalline Anatase (TiO_2)

R. Bouchet,† A. Weibel,† P. Knauth,*,† G. Mountjoy,‡ and A. V. Chadwick‡

MADIREL (UMR 6121), Université de Provence-CNRS, Centre St Jérôme, 13397 Marseille Cedex 20, France, and Functional Materials Group, School of Physical Sciences, University of Kent, Canterbury, Kent CT2 7NR, U.K.

Received July 16, 2003. Revised Manuscript Received October 20, 2003

Segregation of an acceptor (Zn) and a donor dopant (Nb) in nanocrystalline anatase was studied by EXAFS spectroscopy. Different dopant concentrations between 0.1 and 1 at. % were investigated, and similar results were found for nanocrystalline powders and nanocrystalline ceramics made by hot-pressing the powders. Niobium did not segregate whatever the concentration, whereas zinc segregation was found above 0.1 at. %. These results can be interpreted based on defect thermodynamics, in the framework of a space charge segregation model.

1. Introduction

The defect and solute distribution at grain boundaries influences many properties of polycrystalline materials, including grain boundary energy, grain growth, fracture and deformation, or transport properties, such as diffusion along or conductivity across grain boundaries. This influence can become particularly important for properties of materials with reduced dimensions, such as very thin films or nanocrystalline solids, which are currently being rapidly developed in the framework of nanotechnology.[1] There is now sufficient experimental evidence showing that grain boundaries in nanocrystalline materials are structurally similar to those in conventional bulk solids and without the particular disorder invoked in early studies.[2] Nevertheless, although the nature of the grain boundaries is unchanged, their density is extremely high, affecting the electrical and mechanical properties of nanocrystalline materials. The boundaries can also act as dopant or impurity sinks, where considerable amounts can segregate, leading to apparently large dopant or impurity solubility. In Cu-doped CeO_2, Cu segregation can be used to improve the catalytic activity.[3] Furthermore, the catalytic properties of small nanocrystallites are modified by the particular surface morphology with absence of surface faceting.[4] In Gd-doped CeO_2, the observed electrical properties have been attributed to "undoping" of nanocrystallites by grain-boundary Gd segregation.[5] These few examples show that dopant segregation in nanocrystalline oxides is not only a challenging subject for fundamental study, but they also present clear implications for practical work. The key to understanding is a detailed knowledge of atomic level microstructure.

Titanium dioxide is a model binary oxide for fundamental studies that presents many of the exciting properties of electroceramics, including variations of oxygen stoichiometry and ranges of ionic or electronic conductivity.[6] It can also be readily doped with acceptor or donor dopants, i.e., solutes with negative or positive effective charge, respectively. TiO_2 has a multitude of applications: it has been a grand-scale white pigment for many years and is currently under investigation for advanced technological and environmental applications, such as solid-state gas sensors,[7] photovoltaic cells,[8] and photocatalysis.[9] The metastable anatase modification presents better characteristics for photoelectrochemistry. Concerning the defect properties of TiO_2, there is still ongoing debate as to whether Schottky or cation Frenkel disorder is predominant. A good piece of evidence was recently brought forward to make the case for cation Frenkel-type disorder, with titanium interstitials and titanium vacancies as predominant defects. This model allows interpretation of Ti diffusion in rutile single crystals[10] and $P(O_2)$-dependent electrical conductivity of nominally undoped nanocrystalline anatase.[6] Under reducing conditions, the reduction reaction of TiO_2 can be written with partially ionized titanium interstitials, using Kröger−Vink nomenclature:[6]

$$TiO_2 = Ti_i^{\bullet\bullet} + O_2(g) + 2e' \qquad (1)$$

A significantly lower reduction energy in comparison with conventional rutile TiO_2 (7.8 vs 10 eV) was deduced

* Corresponding author. Tel: +33 491 637 114. E-mail: knauth@up.univ-mrs.fr.
† MADIREL.
‡ University of Kent.

(1) Gleiter, H. *Acta Mater.* **2000**, *48*, 1−29.
(2) Chadwick A. V.; Rush, G. E. Characterization of nanocrystalline oxides by EXAFS spectroscopy. In *Nanocrystalline Metals and Oxides: Selected Properties and Applications*; Knauth, P., Schoonman, J., Eds.; Kluwer: Boston, MA, 2002; pp 133−164.
(3) Knauth, P.; Schwitzgebel, G.; Tschöpe, A.; Villain, S. *J. Solid State Chem.* **1998**, *140*, 295−299.
(4) Stark J. V.; Klabunde K. J. *Chem. Mater.* **1996**, *8*, 1913−1918.
(5) Chiang, Y.-M.; Lavik, E. B.; Blom, D. *Nanostruct. Mater.* **1997**, *9*, 633−642.
(6) Knauth, P.; Tuller, H. L. *J. Appl. Phys.* **1999**, *85*, 897−902.
(7) Ferroni, M.; Carotta, M. C.; Guidi, V.; Martinelli, G.; Ronconi, F.; Sacerdoti, M.; Traversa, E. *Sens. Actuators, B* **2001**, *77*, 163−166.
(8) O'Regan B.; Grätzel, M. *Nature* **1991**, *353*, 737−740.
(9) Sakkas, V. A.; Albanis, T. A. *Appl. Catal., B* **2003**, *46*, 175−188.
(10) Hoshino, K.; Peterson, N. L.; Wiley: C. L. *J. Phys. Chem. Solids* **1985**, *46*, 1397−1411.

10.1021/cm034640n CCC: $25.00
Published on Web 11/21/2003

from the temperature dependence of anatase conductivity data, which reflects the greater facility of defect formation at interface sites. This conclusion is supported by various experimental and theoretical studies (see, e.g., refs 11 and 12). In the following, we will consistently consider Frenkel cation disorder as predominant in nanocrystalline anatase.

Two modes of segregation are encountered in ionic materials. The first one is common with metallic systems and is due to ionic radius misfit between host and solute ion. The second one, the possibility of existence of space charge regions with redistribution of charged defects in both the boundary core and the adjacent space charge zones, is particular to semiconductors and ionic compounds. This phenomenon was first discussed for free surfaces,[13] but occurs also at other interfaces, including grain boundaries.[14] There are experimental observations on a number of systems, including titanium dioxide in the rutile phase.[15,16] At elevated temperature, Al and Nb segregation are clearly detected by scanning transmission electron microanalysis. [16] In anatase samples at lower temperature, Nb segregation is observed only before and during phase transition into the rutile phase.[17]

Another important technique for studying the nature of grain boundaries and the position of impurity atoms in nanocrystalline oxides is extended X-ray absorption fine structure (EXAFS) spectroscopy.[2] Major advantages of this method are its nondestructive nature, its sensitivity to low atomic concentrations, and the ability to provide quantitative information on the local environment of atoms, such as radial distances or coordination numbers, without the necessity of long-range order. However, the intensity of EXAFS oscillations depends on the mass of the backscattering atom and the technique is more appropriate for heavy elements. Previous EXAFS investigations have been focused on nanocrystalline oxide powders or thin-films.

We present in the following an EXAFS study of dopant segregation in nanocrystalline anatase TiO_2 powders, but also, for the first time, in a nanocrystalline anatase ceramic, i.e., a dense three-dimensional solid with a mean grain size in the nanometer range, made by hot-pressing the powdered precursor. One of the objectives of this study is to reveal possible differences between segregation at powder surfaces and ceramic grain boundaries. Another is to investigate for the first time a phase-pure nanocrystalline anatase ceramic, which is particularly difficult to achieve, given the phase transition into the stable rutile structure that is normally observed during powder processing at elevated temperature. The investigated dopants are an acceptor, zinc, and a donor, niobium, with a sufficiently high mass.

(11) Chiang, Y.-M.; Lavik, E. B.; Kosacki, I.; Tuller, H. L.; Ying, J. Y. *J. Electroceram.* **1997**, *1*, 7−14.
(12) Balducci, G.; Kaspar, J.; Fornasiero, P.; Graziani, M.; Islam, M. S. *J. Phys. Chem. B* **1998**, *102*, 557−561.
(13) Lehovec, K. *J. Chem. Phys.* **1953**, *21*, 1123−1128.
(14) Maier, J. *Prog. Solid State Chem.* **1995**, *23*, 171−263.
(15) Ikeda, J. A. S.; Chiang, Y.-M. *J. Am. Ceram. Soc.* **1993**, *76*, 2437−2446.
(16) Ikeda, J. A. S.; Chiang, Y.-M.; Garratt-Reed, A. J.; Vander Sande, J. B. *J. Am. Ceram. Soc.* **1993**, *76*, 2447−2459.
(17) Arbiol, J.; Cerdà, J.; Dezanneau, G.; Peiro, F.; Cornet, A.; Morante, J. R. *J. Appl. Phys.* **2002**, *92*, 853.

Table 1. Chemical Analyses and BET Surface Areas of TiO_2 Powders Calcined at 600 °C

% Zn	% Nb	% SO_4	Na/ppm	BET/m^2 g^{-1}
<5 ppm	0.04	0.21	200	49
0.11	0.04	0.21	200	60
0.47	0.04	0.24	<100	48
1.0	0.04	0.24	<100	51
9 ppm	0.1	0.24	<100	50
<5 ppm	0.4	0.24	<100	62
<5 ppm	1.0	0.24	<100	63

2. Experimental Section

Nanocrystalline phase-pure anatase was prepared by precipitation from sulfuric acid solutions by addition of sodium hydroxide. Accordingly, nominally undoped TiO_2 contains as major impurities Na (0.02 mol %), acting as acceptor, and S (0.21 mol %), present as sulfate ions dissolved in the bulk on anion sites. The amount of zinc (<5 ppm) and niobium (400 ppm) was also determined. The dopants were added and intensely mixed after precipitation. The precipitates were thoroughly washed and calcined for 1 h at 300, 450, or 600 °C. The average grain size was estimated on the basis of the Scherrer equation using the width at half-maximum of (*hkl*) X-ray diffraction peaks. Similar size (≈20 nm) was deduced from the reflections of different (*hkl*) values, suggesting that the crystallites were of a regular shape. The chemical analyses and the BET surface areas of TiO_2 powders calcined at 600 °C are presented in Table 1.

Nanocrystalline anatase ceramics were made by hot-pressing the powders calcined at 600 °C. In this procedure, the powder was introduced in pure alumina dies, compressed under 6000 bar and then subjected to a fixed heating rate of 10 K/min up to a plateau temperature of 600 °C, where it was kept for 2 h, before the pressure was released and the ceramic was cooled with the intrinsic cooling rate of the hot-press (Cyberstar, Grenoble). The density of the nanocrystalline ceramics was determined from mass and geometrical dimensions and confirmed by dilatometric experiments and mercury porosimetry. Densities of (92 ± 1)% of theory, based on the density of pure anatase, were obtained under these conditions.

The EXAFS data were collected at the Daresbury Synchrotron Radiation Source. Ti K-edge EXAFS spectra were recorded in transmission mode at room temperature on station 7.1. The synchrotron has an electron energy of 2 GeV and the average current during the measurements was 150 mA. Anatase TiO_2 powders were pressed into pellets with nonabsorbing polyethene as diluent. For the nanocrystalline anatase ceramics, EXAFS spectra were obtained in fluorescence mode at station 9.3. This mode was also used to collect K-edge EXAFS data for the dopant elements, Zn and Nb. Station 9.3 allows simultaneous determination of X-ray diffraction patterns; it is also equipped with a furnace so that spectra can be recorded at temperatures between ambient and 1100 °C and the effect of heating on particle size can be monitored. EXAFS data analysis was performed with EXCALIB, EXBACK, and EXCURV98 computer programs developed at the Daresbury synchrotron.[2] Phase shifts were derived from ab initio calculations within EXCURV98. This code also includes routines to treat multiple scattering effects in highly symmetric structures. For each spectrum a theoretical fit was obtained by adding shells of atoms around the central excited atom and least-squares iterating the edge position, E_o, radial distances, RD, and the Debye−Waller type factors, A ($= 2\sigma^2$). This latter factor will contain contributions from both thermal disorder and static variations in RD. The coordination number, CN, can also be iterated. The quality of the fit is measured by an *R*-factor and the errors in RD are ∼±0.02 Å and ∼±20% in *A* and CN.

3. Results

Typical Ti K-edge EXAFS spectra and the corresponding Fourier transforms of the data for TiO_2 are

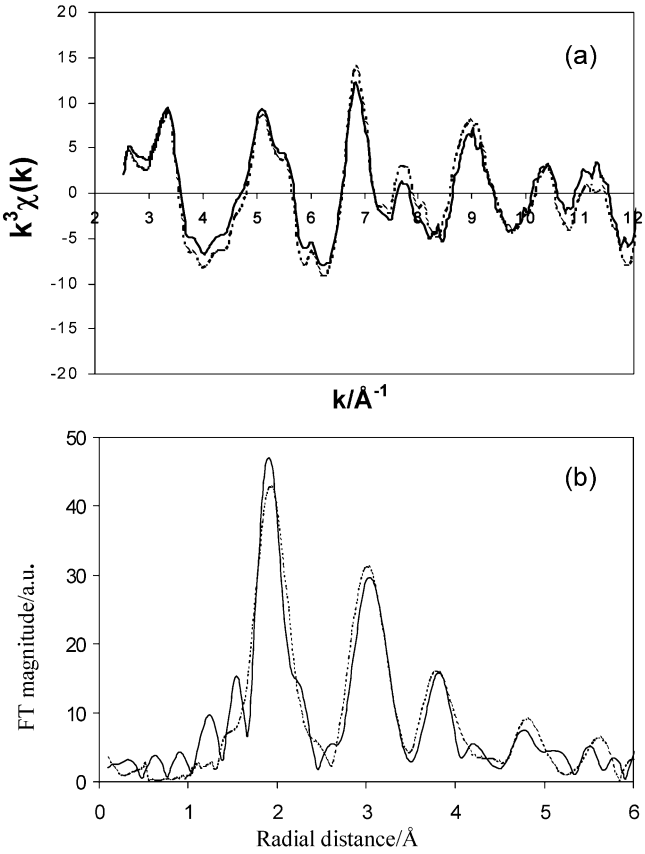

Figure 1. Ti K-edge EXAFS spectra (k^3-weighted) and corresponding Fourier transforms for TiO_2; (a) normalized EXAFS and (b) the corresponding Fourier transform corrected with the phase shift of the first shell. The experimental data for nanocrystalline TiO_2 are represented by the solid line and the data for bulk anatase are the dotted line. The best fit parameters for the EXAFS are given in Table 2.

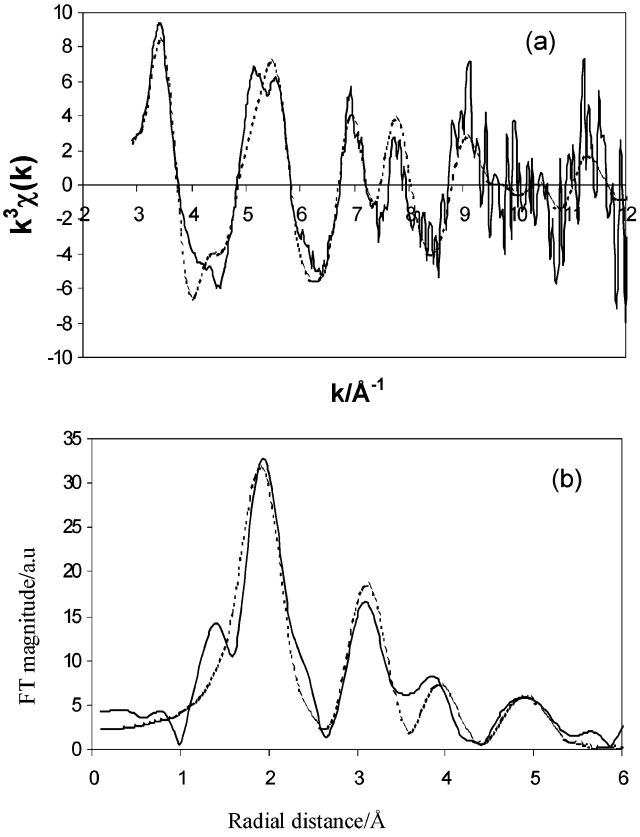

Figure 2. Nb K-edge EXAFS spectra (k^3-weighted) and corresponding Fourier transforms for 1%-Nb-doped TiO_2 sample after heating at 600 °C; (a) the normalized EXAFS and (b) the corresponding Fourier transform corrected with the phase shift of the first shell. The experimental data are the solid line and the best fit is the dotted line. The best fit parameters for the EXAFS are given in Table 3.

shown in Figure 1. The solid line represents the data for the nanocrystalline and the dashed line is the data for bulk anatase. One notices a good agreement between the two spectra. There are three major peaks in the Fourier transforms corresponding to shells of O atoms (∼2 Å), Ti atoms (∼3 Å), and a mixed shell of O and Ti atoms (∼3.8 Å). The data were least-squares fitted, with E_o, RD, and A as variable parameters, with EXCURV98, and the best-fit parameters are shown in Table 2. The crystallographic data were used as the starting model and the coordination numbers were held constant. The fitting was extended out to 5 Å to test the reliability of the parameters. There is a good agreement (within the expected error for the EXAFS data) between the RD values from the EXAFS and crystallographic data for the first three shells. The agreement is less good, as expected, for outer shells which contain a mixture of O and Ti atoms at similar distances. The Debye−Waller factors for the outer shells are significantly larger for the nanocrystalline sample and may reflect a particle size effect.

A typical fluorescence Nb K-edge EXAFS spectrum of 1% Nb-doped anatase powders calcined at 600 °C is shown in Figure 2. There are clear similarities between this spectrum and the Ti K-edge spectrum shown in Figure 1: the three main peaks in the Fourier transform occur at similar distances and have roughly the same relative magnitudes. In addition, the spectrum is very different from the Nb K-edge spectrum of pure Nb_2O_5, shown for comparison in Figure 3. The local environment of Nb^{5+} in Nb_2O_5 is a highly distorted octahedron of O^{2-} ions at radial distances ranging from 1.72 to 2.28

Table 2. Best-Fit Parameters to the Ti K-Edge EXAFS

	TiO_2 XRD		EXAFS Nanocrystalline TiO_2			EXAFS Bulk TiO_2		
atom	CN	RD/Å	CN	RD/Å	A/Å^2	CN	RD	A/Å^2
O	4	1.934	6	1.923	0.019	6	1.935	0.014
O	2	1.979						
Ti	4	3.039	4	3.026	0.016	4	3.033	0.012
Ti	4	3.785	4	3.866	0.017	4	3.789	0.025
O	8	3.856	8	3.969	0.022	8	3.802	0.017
O	8	4.250	16	4.568	0.065	16	4.614	0.064
O	8	4.271						
O	4	4.751	4	4.858	0.058	4	4.914	0.025
Ti	8	4.854	8	4.808	0.031	8	4.822	0.024
			E_o = 3.08 eV; R = 34.8%			E_o = 2.75 eV; R = 27.6%		

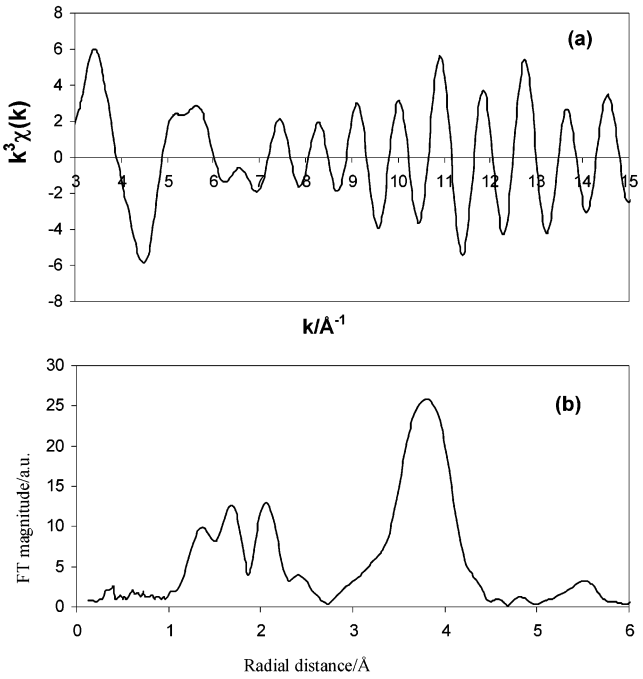

Figure 3. Nb K-edge EXAFS spectra (k^3-weighted) and corresponding Fourier transforms for pure Nb_2O_5; (a) the normalized EXAFS and (b) the corresponding Fourier transform corrected with the phase shift of the first shell.

Å and the EXAFS is dominated at high k by the strong Nb−Nb correlation. Examination of the three spectra in Figures 1, 2, and 3 is strong evidence that the Nb ions in the 1% Nb-doped anatase powders are predominantly in substitutional sites in the TiO_2 lattice. The EXAFS for all the Nb-doped anatase were all fitted on this basis; the Nb^{5+} was on the Ti^{4+} site, and E_o, RD, and A were iterated to a best-fit. The parameters are listed in Table 3. Only the values for the first three shells are listed, as in the case of pure TiO_2 parameters for higher shells are less meaningful. One notices, in general, that peak amplitudes, Debye−Waller factors, and distances for the first O coordination shell are similar to those found for pure TiO_2. The most significant feature is a consistently higher distance for the Ti shells as compared with that of bulk anatase. This may reflect the stronger Coulombic repulsion between near neighbor Nb^{5+} and Ti^{4+} ions compared to that between Ti^{4+} and Ti^{4+} ions.

Fourier transforms of EXAFS data are compared for 1% Nb-doped powders calcined at 300 and 600 °C and a nanocrystalline ceramic sample in Figure 4. One notices no significant differences between the three samples and, more importantly, the presence of several peaks corresponding to Nb−O and Nb−Ti correlations. The raw data for the nanoceramic were less good than

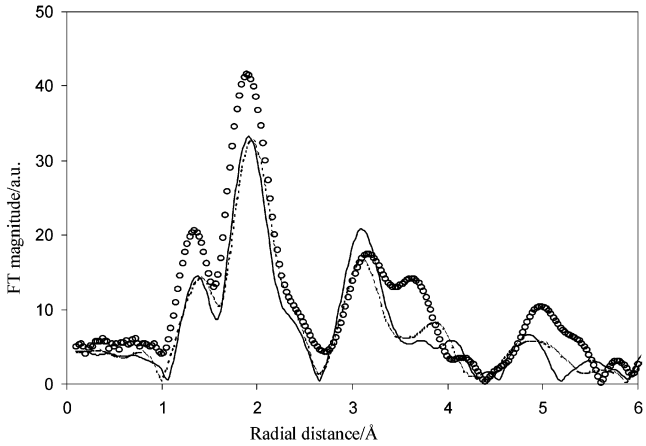

Figure 4. Fourier transforms of the Nb K-edge EXAFS data for 1% doped samples of TiO_2. The solid line is for sample heated at 300 °C, the dashed line is for the sample heated at 600 °C, and the circles are for the nanoceramic.

those for the powders, and this accounts for some of the differences in the shells beyond the first two. The radial distances and Debye−Waller factors obtained from the detailed fitting for the first three shells with coordination numbers fixed at those of bulk anatase are given in Table 3. From these data and a comparison with bulk anatase, it is quite clear that Nb atoms predominantly occupy substitutional Ti bulk sites in all the samples. There is no indication for significant Nb segregation either at surfaces of anatase nanoparticles or at grain boundaries of anatase nanoceramics. A similar conclusion can be drawn for lower Nb concentrations (0.1 and 0.5 mol %). To check the influence of a prolonged heating on segregation kinetics, a sample was also pressed and calcined at 600 °C for 10 h. However, this treatment did not change significantly the reported results and there was no evidence for interfacial dopant segregation after heating.

For the Zn-doped samples, the results are more complicated. A typical fluorescence Zn K-edge EXAFS spectrum of 1% Zn-doped anatase calcined at 600 °C is shown in Figure 5. Fourier transforms of EXAFS data for 1% Zn-doped powders calcined at 300 and 600 °C and a nanoceramic sample are compared in Figure 6. The radial distances and Debye−Waller factors obtained from the detailed fitting of the first three shells with coordination numbers fixed at those of bulk anatase are given in Table 3. After the strong Zn−O peak with a radial distance corresponding to bulk anatase (and also the Zn−O distance in ZnO), all 3 samples show a very small magnitude of the second peak amplitude corresponding to the Zn−Ti correlation. This is reflected in the very large Debye−Waller factors for the Zn−Ti shells, particularly for the first Zn−Ti shell, which are

Table 3. Best-Fit Parameters to the Dopant K-Edge EXAFS

		Ti EXAFS nanocrystalline powder		Nb EXAFS in 1% Nb-dopedTiO_2						Zn EXAFS in 1% Zn-dopedTiO_2						Zn EXAFS in 0.1% Zn-dopedTiO_2			
				300°C		600°C		ceramic		300°C		600°C		ceramic		300°C		600°C	
atom	CN	R/Å	A/Å^2	R/Å	A/Å^2	R/Å	A/Å^2	R/Å	A/Å^2	R/Å	A/Å^2	R/Å	A/Å^2	R/Å	A/Å^2	R/Å	A/Å^2	R/Å	A/Å^2
O	6	1.923	0.019	1.947	0.012	1.963	0.022	1.947	0.008	1.989	0.025	1.973	0.029	1.969	0.029	1.977	0.029	1.988	0.022
Ti	4	3.026	0.016	3.112	0.015	3.112	0.019	3.128	0.017	2.713	0.147	3.313	0.068	2.632	0.105	3.031	0.034	3.038	0.027
Ti	4	3.866	0.017	3.951	0.027	3.932	0.023	3.918	0.028	3.834	0.035	3.836	0.048	3.879	0.070	3.831	0.025	3.816	0.023
		E_o = 3.08 eV; R = 34.8%		E_o = 5.80 eV; R = 38.0%		E_o = 5.81 eV; R = 39.5%		E_o = 5.78 eV; R = 38.6%		E_o = −1.92 eV; R=39.2%		E_o =− 1.58 eV; R = 39.8%		E_o = −1.41 eV; R = 39.7%		E_o = −1.78 eV; R = 34.8%		E_o = −1.38 eV; R = 35.1%	

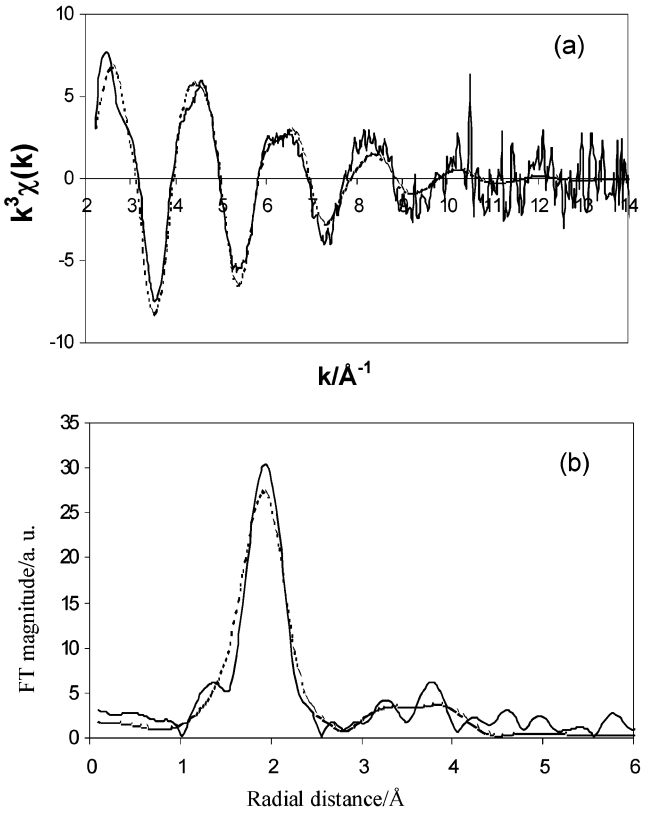

Figure 5. Zn K-edge EXAFS spectra (k^3-weighted) and corresponding Fourier transforms for 1%-Zn-doped TiO_2 sample after heating at 600 °C; (a) the normalized EXAFS and (b) the corresponding Fourier transform corrected with the phase shift of the first shell. The experimental data are represented by the solid line and the best-fit is the dotted line. The best-fit parameters for the EXAFS are given in Table 3.

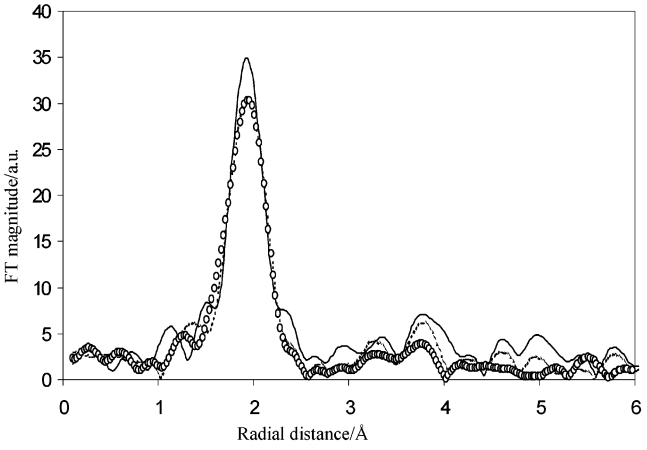

Figure 6. Fourier transforms of the Zn K-edge EXAFS data for 1% doped samples of TiO_2. The solid line is for sample heated at 300 °C, the dashed line is for the sample heated at 600 °C, and the circles are for the nanoceramic.

much larger than those for the corresponding Nb−Ti values in the Nb-doped samples. Attempts were made to fit the data with the CNs as additional variable parameters. These were unsuccessful and led to meaningless parameters, i.e., coordination numbers much less than unity and negative Debye−Waller factors. In comparison to similar studies of doped oxides (for example, Cu- and Fe-doped SnO_2[18]), the simplest explanation is that the Zn atoms are segregated at the boundary. In such a situation the Zn ions will be closely surrounded by a shell of O ions but outer shells will be disordered.

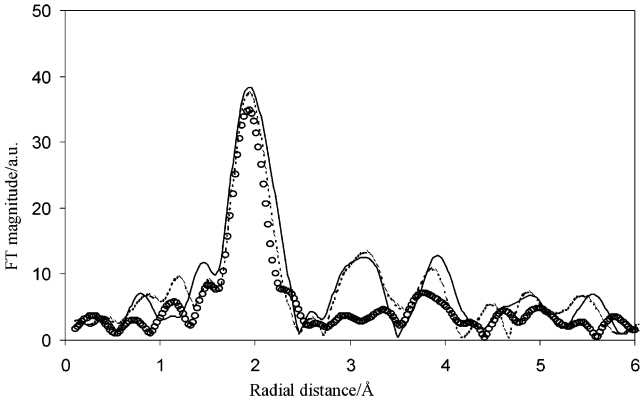

Figure 7. Fourier transforms of the Zn K-edge EXAFS data for 0.1% doped samples of TiO_2. The solid line is for sample heated at 300 °C, the dashed line is for the sample heated at 600 °C. For comparison the 1%-Zn-doped sample heated at 300 °C is shown as circles.

We have also investigated the Zn concentration-dependence of segregation. At the lowest investigated concentration of 0.1 mol % Zn, there is evidence from the EXAFS that the dopant is at least partially dissolved on regular Ti bulk positions. This can be observed in Figure 7 for samples calcined at 300 and 600 °C. In both cases, after the dominant peak around 2 Å, two further peaks can be observed around 3.0 and 3.8 Å, corresponding to significant Zn−Ti correlations, comparable to the Nb−Ti correlations in the Nb-doped samples. The radial distances and Debye−Waller factors obtained from the analysis of the EXAFS data are reported in Table 3. The 0.5 mol % Zn-doped samples show an intermediate behavior: segregation is observed for powders calcined at 600 °C, which present a larger particle size. The peaks corresponding to Zn−Ti correlations are, however, clearly visible for the sample calcined at 300 °C. The simplest explanation is that the Zn bulk solubility is between 0.1 and 0.5 mol % and that annealing leads to Zn segregation.

4. Discussion

Can we now give a consistent explanation for the clear Zn segregation and the absence of Nb segregation in nanocrystalline anatase? Let us recall the basic driving forces for boundary segregation.

First, ion radius mismatch creates strains and stresses around a dopant ion that can be reduced if the dopant leaves the regular lattice and segregates to a boundary where the free volume is normally different from that in the bulk. The corresponding segregation isotherm can usually be described by the McLean−Guggenheim equation, similar to the one derived for metallic systems.[19] However, this equation assumes electroneutral segregation, which is often not a good postulate in ionic systems. Considering the ionic radii in our system, using the data tabulated for octahedral environment (Pauling radii) in refs 20 and 21, Zn^{2+} (0.74 Å) and Nb^{5+} ions

(18) Davis, S. R.; Chadwick, A. V.; Wright, J. D. *J. Phys. Chem. B.* **1997**, *101*, 9901−9908.
(19) McLean, D. *Grain Boundaries in Metals*; Clarendon: Oxford, U.K., 1957.

(0.69 Å) have a radius quite similar to that of the host Ti^{4+} ion (0.68 Å). Other ion valences, such as Ti^{3+} or Nb^{4+}, are only relevant under strongly reducing conditions, not encountered in our study. The mechanical energy can be estimated using empirical laws[16] to be below 0.1 eV. This mode of segregation is therefore clearly unimportant in our system.

Second, electrostatic interactions between charged defects and ionized dopants lead to space charge segregation. In this case, the segregation isotherm must be written introducing explicitly a boundary potential $\phi(0)$. This electrostatic driving force is much more relevant for our problem. It is well-known that the boundary potential of most undoped oxides, such as TiO_2, is positive, corresponding to a positive boundary charge due to easy boundary reduction and formation of an oxygen deficiency at the boundary core. It is important to emphasize here the difference with the space charge model assumed for explaining the sensor characteristics of rutile TiO_2 for reducing gases. In that model, the oxygen deficiency of TiO_2 is not considered and a negative surface charge due to chemisorbed oxygen ions, such as O^-, is assumed. However, the relevance of an oxygen deficiency for most nanocrystalline oxide surfaces has been shown in several recent investigations, and positive boundary potentials were reported for various oxides, including CeO_2 [22,23] and ZrO_2.[24]

In the case of nominally undoped anatase and considering predominant cation Frenkel disorder, a positive boundary charge corresponds to a boundary excess of positive titanium interstitials, in other words a point defect segregation process, written with twice-ionized titanium interstitials (the ionization state does not change the qualitative conclusions):

$$Ti_i^{\bullet\bullet} + V_B = V_i + Ti_B^{\bullet\bullet} \quad (2)$$

In this equation, boundary sites are written using a subscript B: $Ti_B^{\bullet\bullet}$ is an excess titanium ion at a boundary and V_B is an initially empty boundary site. The corresponding mass action law can be obtained by assuming local thermodynamic defect equilibrium. This yields a relation:

$$\mu(Ti_B^{\bullet\bullet}) + \mu(V_i) - \mu(Ti_i^{\bullet\bullet}) - \mu(V_B) = -2F\phi(0) \quad (3)$$

where μ represents the chemical potential and F is Faraday's constant (for molar quantities). By definition, the bulk potential is taken as zero. The segregation constant can be written as follows:

$$K_{seg}(Ti_i) \approx [Ti_B^{\bullet\bullet}]/[Ti_i^{\bullet\bullet}] = \exp - [\Delta G^B(V_i) + \Delta G^B(Ti_i^{\bullet\bullet}) + 2F\phi(0)]/RT \quad (4)$$

where R is the gas constant and T is the absolute temperature. Here, we assume for simplicity that the concentration of vacant interstitial bulk and vacant interfacial sites is similar, so that $[V_i] \approx [V_B]$. The standard chemical potentials are defined as follows:

$$\Delta G^B(Ti_i^{\bullet\bullet}) = \mu^\circ(Ti_B^{\bullet\bullet}) - \mu^\circ(Ti_i^{\bullet\bullet}) \quad (5)$$

$$\Delta G^B(V_i) = \mu^\circ(V_i) - \mu^\circ(V_B) \quad (6)$$

As one can easily recognize, the boundary potential $\phi(0)$ depends decisively on the difference between the standard chemical potentials of titanium interstitials in the bulk and at interfaces. Overall charge neutrality in the system implies that negatively charged counter defects of the positive boundary charge, i.e., titanium vacancies and electrons, are accumulated in the space charge regions adjacent to the boundary, whereas positively charged defects, including titanium interstitials and electron holes, are depleted.

In doped systems, cosegregation of point defects and dopants can occur, corresponding for niobium- and zinc-doped samples to the following reactions:

$$Nb_{Ti}^{\bullet} + Ti_i^{\bullet\bullet} = Nb_B^{\bullet} + Ti_B^{\bullet\bullet} \quad (7)$$

$$K_{seg}(Nb) \approx [Nb_B^{\bullet}][Ti_B^{\bullet\bullet}]/[Nb_{Ti}^{\bullet}][Ti_i^{\bullet\bullet}] = \exp - [\Delta G^B(Ti_i^{\bullet\bullet}) + \Delta G^B(Nb_{Ti}^{\bullet}) + 3F\phi(0)]/RT \quad (8)$$

$$\Delta G^B(Nb_{Ti}^{\bullet}) = \mu^\circ(Nb_B^{\bullet}) - \mu^\circ(Nb_{Ti}^{\bullet}) \quad (9)$$

$$Zn_{Ti}^{\bullet\bullet} + Ti_i^{\bullet\bullet} = Zn_B^{\bullet\bullet} + Ti_B^{\bullet\bullet} \quad (10)$$

$$K_{seg}(Zn) \approx [Zn_B^{\bullet\bullet}][Ti_B^{\bullet\bullet}]/[Zn_{Ti}^{\bullet\bullet}][Ti_i^{\bullet\bullet}] = \exp - [\Delta G^B(Ti_i^{\bullet\bullet}) + \Delta G^B(Zn_{Ti}^{\bullet\bullet})]/RT \quad (11)$$

$$\Delta G^B(Zn_{Ti}^{\bullet\bullet}) = \mu^\circ(Zn_B^{\bullet\bullet}) - \mu^\circ(Zn_{Ti}^{\bullet\bullet}) \quad (12)$$

The negligible difference of ionic radii indicates a small or negligible difference of the standard chemical potentials for dopant ions between bulk and interface sites: $\Delta G^B(Nb_{Ti}^{\bullet}) = \Delta G^B(Zn_{Ti}^{\bullet\bullet}) \approx 0$. One can reasonably assume that at dopant concentrations below 1 mol % considered here, the standard chemical potentials of defects are independent of the nature of the dopant, i.e., $\Delta G^B(Ti_i^{\bullet\bullet})$ is constant. One obtains then, by comparison of eqs 4, 8, and 11, immediately the relation

$$K_{seg}(Zn) > K_{seg}(Ti_i) > K_{seg}(Nb) \quad (13)$$

One can notice a qualitative agreement with the experiment. For a quantitative comparison, more thermodynamic data on defect formation in the bulk and at boundaries in anatase are needed. One can, however, give a plausible explanation for the remarkable absence of Nb segregation in anatase samples at low temperature, observed by us and other authors.[17] According to our electrostatic model of segregation, this is not a kinetic effect, due, e.g., to insufficient thermal activation for Nb migration, but a thermodynamic effect. In the more dense rutile phase, it is reasonable to estimate

(20) *Handbook of Chemistry and Physics*, 61st ed.; Weast, R. C., Ed.; CRC Press: Boca Raton, FL, 1981; p. F216.

(21) Huheey, J. E.; Keiter, E. A.; Keiter, R. L. *Inorganic Chemistry: Principles of Structure and Reactivity*, 4th ed.; Harper-Collins: New York, 1993.

(22) Tschöpe, A. *Solid State Ionics* **2001**, *139*, 267−280.

(23) Tschöpe, A. Space Charge Layers in Polycrystalline Cerium Oxide. In *Solid State Ionics 2002*; Knauth, P., Tarascon, J.-M., Traversa, E., Tuller, H. L., Eds.; MRS Proceedings Volume 756; Materials Research Society: Warrendale, PA, 2003; p 33.

(24) Guo, X.; Sigle, W.; Fleig J.; Maier, J. *Solid State Ionics* **2002**, *154−155*, 555−561.

that the value of $\Delta G^B(Ti_i^{\bullet\bullet})$ will be larger, because interstitial formation in the bulk will be more difficult, driving a measurable segregation also for Nb, as observed experimentally.[16]

5. Conclusion

EXAFS spectroscopy performed on nanocrystalline anatase TiO_2 powder and a nanocrystalline anatase ceramic gives clear indication for Zn segregation, but Nb segregation is not observed, in qualitative agreement with earlier results. The results obtained for surface segregation (in anatase powders) and grain boundary segregation (in anatase nanoceramics) are similar. This behavior is compatible with a space charge segregation model, assuming a positively charged interface core, due to easy interface reduction leading to excess titanium interstitials. According to our results, the boundary potential for a "free" surface is comparable to that for a grain boundary. The absence of Nb segregation in anatase is not a kinetic effect, but can be interpreted considering defect thermodynamics.

Acknowledgment. This work was supported by the EU program, which provided the beam time at the Daresbury SRS. We thank the Daresbury EXAFS station managers, particularly Ian Harvey, Fred Mosselmans, and Lorrie Murphy, for their assistance with the experiments.

CM034640N